19th AIAA Computational Fluid Dynamics
22 - 25 June 2009, San Antonio, Texas

AIAA 2009-3800

DNS of Detonation Wave and Isotropic Turbulence Interaction

Hari Narayanan Nagarajan*, Luca Massa† and Frank K. Lu‡
Aerodynamics Research Center, University of Texas at Arlington, Arlington, TX 76019, USA

A direct numerical simulation of detonation wave with compressible homogeneous isotropic turbulence is carried out with three different detonation Mach numbers to study the effect of detonation wave on turbulence and vice versa. The analysis is based on the integration of the three dimensional chemically reactive Navier–Stokes equations using a Runge–Kutta scheme and a fifth-order WENO spatial discretization. The interaction of the detonation wave and turbulence resulted in higher amplification of the turbulent statistical parameters (such as, turbulent kinetic energy, Taylor length scale and Kolmogorov length scale, rms of the velocity, pressure and thermodynamic parameters) than those observed in the shock-turbulence interaction case. The study also revealed that the amplification of turbulence statistics is proportional to the heat release and activation energy.

I. Introduction

The detonation–turbulence interaction problem is concerned with the unsteady coupling between convected vortical structures and a detonation wave. The dynamics of the interaction reveals the role of noise on detonation wave stability. A much more common type of interaction is the shock–turbulence coupling problem. Lee et al.[1] recently analyzed the coupling and found that the nonlinear problem agrees well with Ribner's linear interaction theory.[2] However, detonation–turbulence interaction is different from shock–turbulence interaction because of the role of the induction region in the amplification of convected vortical structures. Linear analysis[3] shows that the post-shock energy spectra are maximally amplified by the resonant interaction in the induction region. Linear analysis can provide useful insights but fails to correctly represent the system dynamics near natural frequencies.

Powers[4] discussed the multiscale modeling aspects of a detonation wave along with results generated using single-step kinetics for the chemical reaction, emphasizing the necessity of capturing finer scales. A similar technique with one-step kinetics is used for the present work. The pre-shock turbulent field is incompressible, isotropic and chemically homogeneous. The post-shock field is strongly inhomogeneous because of the thermo-fluid coupling in the induction region. Ribner et al.[5] states that the effect of exothermicity is to amplify the rms fluctuations downstream of the detonation, with the greatest changes occurring around the Chapman–Jouguet Mach number with a restrictive assumption of the reaction zone thickness being much smaller than the turbulence length scale (but induction zones can be quite large). A detailed study of the influence of transverse waves on detonation and the pattern of quasi-steady detonation fronts was performed by Dou et al.[6] The dynamics of small fluid-mechanics scales is vital for resolving the thermo-fluid interaction in the induction region of a detonation. An unstable detonation wave possesses a large set of intrinsic fluctuating frequencies with a range that increases with the activation energy.[3]

The paper is organized as follows. In §II, the governing equations and the computational setup are described, followed in §III by a presentation of the validation tests and its results. The DNS of interaction of detonation wave and turbulence is presented and discussed in §IV, in which the general features of the

*Graduate Research Assistant, Mechanical and Aerospace Engineering Department, Student Member AIAA.
†Assistant Professor, Mechanical and Aerospace Engineering Department.
‡Professor, Mechanical and Aerospace Engineering Department, Associate Fellow AIAA.

Copyright © 2009 by the American Institute of Aeronautics and Astronautics, Inc. All rights reserved.

flow field is presented as well as the analysis of the turbulence amplification on several parameters. Finally, in §V, conclusions are drawn.

II. Governing equations

The governing equations are the nondimensional conservative form of the continuity, momentum and energy equations in Cartesian coordinates. The working fluid is assumed to be a perfect gas.

$$\frac{\partial \rho}{\partial t} + \frac{\partial}{\partial x_j}(\rho u_j) = 0 \tag{1a}$$

$$\frac{\partial}{\partial t}(\rho u_i) + \frac{\partial}{\partial x_j}(\rho u_i u_j + p\delta_{ij} - \sigma_{ij}) = 0, \quad i = 1, 2, 3 \tag{1b}$$

$$\frac{\partial E}{\partial t} + \frac{\partial}{\partial x_j}(E u_j + u_j p + q_j - u_i \sigma_{ij}) = 0 \tag{1c}$$

$$\frac{\partial \rho Z}{\partial t} + \frac{\partial}{\partial x_j}(\rho Z u_j) = (\rho - \rho Z) r(T) \tag{1d}$$

The nondimensionalization is obtained using the equations given below, for the nonreactive terms,

$$\begin{array}{lll} x_i^* = \frac{x_i}{L} & t^* = \frac{t}{L/V_\infty} & \mu^* = \frac{\mu}{\mu_\infty} \\ \rho^* = \frac{\rho}{\rho_\infty} & T^* = \frac{T}{T_\infty} & e^* = \frac{e}{V_\infty^2} \\ u_i^* = \frac{u_i}{V_\infty} & p^* = \frac{p}{\rho_\infty V_\infty^2} & \end{array} \tag{2}$$

and for the reactive terms are obtained using the following relation

$$Q^* = \frac{Q\rho_\infty}{P_\infty} \quad E^* = \frac{E\rho_\infty}{P_\infty} \quad K_0^* = K_0 \frac{L}{V_\infty} \tag{3}$$

The variable Z is the reaction progress, where $Z = 0$ describes the unburnt state and $Z = 1$ the completely burnt state. Here, the total energy of the fluid is given by

$$E = \rho \left(\frac{P}{\gamma - 1} + \frac{u_i^2}{2} - QZ \right) \tag{4}$$

where Q is the heat release and the term $Q\rho Z$ denotes the chemical energy which is released as heat during the combustion process. The reaction rate $r(T)$ is described by a single–step, Arrhenius law and depends on the temperature T through the relation

$$r(T) = K_0 \exp(-E/T) \tag{5}$$

where K_0 is the pre-exponential factor (also known as rate constant) that sets the temporal scale of the reaction and E is the activation energy. The assumption of a single-step, Arrhenius kinetics law for $r(T)$ has been often employed in numerical studies. The important characteristics of the propagation of detonation waves can be sufficiently described by this simple chemistry model. On the other hand, this simplified model cannot provide an accurate description of the thermochemistry of actual detonations and, therefore, its applicability has certain limitations. Important phenomena, such as detonation initiation or deflagration-to-detonation transitions, require a more detailed reaction mechanism.[7] In what follows the superscript * is dropped from the non-dimensional variables detailed in (2).

II.A. Computational Setup

The one-dimensional version of a weighted essentially non-oscillatory (WENO) Euler code[8] was modified to a three-dimensional WENO Euler code as the initial step and it was subsequently converted to DNS

code. The easiest way to solve a multidimensional problem is by using the dimensional splitting approach. A multidimensional problem is simply split into a sequence of one-dimensional problems and hence uses dimension-by-dimension reconstruction. Dimension-by-dimension reconstruction is simpler and computationally less expensive than the genuine multidimensional approach.[9] Because the implementation of the three-dimensional WENO scheme in the present DNS is identical to that used by Titarev,[8,9] a very brief description is given here. The reconstruction is carried out using the WENO 5^{th}-order scheme.[10–18] Weighted essentially non-ocillatory (WENO) methods have been developed to simultaneously provide robust shock capturing in compressible turbulence fluid flow and avoid excessive damping of fine-scale flow features such as turbulence.[19] The convective numerical fluxes are computed using a 5^{th} order WENO scheme and the viscous fluxes are computed using a sixth order central standard scheme. The time integration is carried out using the third-order Runge–Kutta scheme.

III. Validation of the Three-Dimensional WENO-Based Navier–Stokes Model

Validation of the WENO solver was carried out extensively in different stages of the code development. Initially, one-dimensional version was validated using standard test cases and, subsequently, a three-dimensional version of the same was tested. Salient results of all the validation exercise is discussed below.

III.A. Validation of the One-Dimensional WENO Euler Code

The one-dimensional WENO solver was validated using the Sod's and Lax's problems . In both cases, the computational domain was $[-5, 5]$ and the number of cells N was taken as 500. A zero-order boundary condition was employed. The density trend of the shock shows a reasonably good agreement with the analytical result and corroborated published results for the 5^{th}-order WENO scheme.[10,20] Sod's problems results are not shown here for brevity.

The initial data used for the Lax's problem are given as

$$(\rho, u, P) = \begin{cases} 0.445, 0.698, 3.528 & x < -4 \\ 0.5, 0, 0.571 & x \geq -4 \end{cases}$$

The density trend of the shock wave (Fig. 1) shows good agreement with the analytical result. These trends corroborated published results for the 5^{th}-order WENO scheme.[10]

III.B. Validation of the One-Dimensional WENO Reactive Euler code

Various concepts of pulse detonation engines have been evaluated either theoretically or experimentally during the past several decades.[21–26]

Experimental studies relevant to detonation and pulse detonation engines have been carried out during past several decades.[24,27,28] Some of the experiments were concerned with the structure of detonation.[23,25,29] Experimental results with hydrogen–oxygen detonation also confirmed the existence of the induction zone[21] as postulated by ZND and observed by many others. Numerical studies relevant to detonation also showed considerable progress.[6,7,30–39]

Simulation of the one-dimensional detonation wave is accomplished using the concepts based on the well-known ZND model.[39–41] In this validation, inviscid, non-heat conducting flow is assumed. A simple model of the chemical interaction between two perfect gases $A \rightarrow B$, is obtained using one-step, irreversible Arrhenius kinetics. The pre- and post-detonation conditions are obtained using the Rankine–Hugoniot relations,

$$\rho u = -D\rho_0 \tag{6a}$$

$$\rho u^2 + P = D^2\rho_0 + P_0 \tag{6b}$$

$$\rho u\left(\frac{P}{\rho(\gamma-1)} + QZ + \frac{u^2}{2}\right) + pu = -D\rho_0\left(\frac{P_0}{\rho_0(\gamma-1)} + q_0 + \frac{D^2}{2} + \frac{P_0}{\rho_0}\right) \tag{6c}$$

$$Z = Z_0 \tag{6d}$$

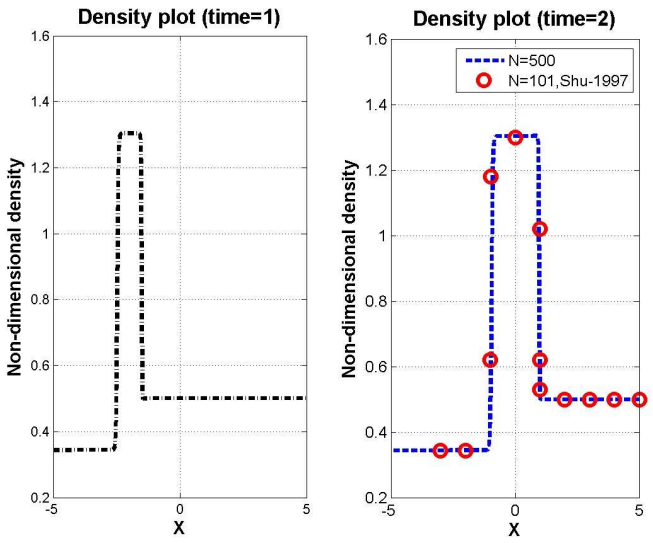

Figure 1. Lax's problem

where variables with subscript 0 refers to the pre-detonation condition. We employ the relationship $Y = 1-Z$. Simplification of Eqs. (6c)–(6d) yields

$$\frac{\gamma}{\gamma-1}\frac{P}{\rho} - q_0\frac{P}{\rho}Y + \frac{u^2}{2} = \frac{\gamma}{\gamma-1}\frac{P_0}{\rho_0} + \frac{u_0^2}{2} \tag{7a}$$

$$Y = Y_0 \tag{7b}$$

These equations are closed by using the definition of the overdrive factor of a ZND detonation, which is defined by

$$f = \left(\frac{D}{D_{CJ}}\right)^2 \tag{8}$$

where D is the detonation velocity and D_{CJ} is the velocity of the corresponding Chapman–Jouguet wave (defined as the detonation in which the gas velocity at the end of the reaction zone, and in the reference frame of the shock, equals to the speed of sound). D_{CJ} is equal to $M_{CJ}\sqrt{\gamma P_0/\rho_0}$, where,

$$M_{CJ}^2 = 1 + \frac{\gamma^2-1}{\gamma}Q + \sqrt{\frac{\gamma^2-1}{\gamma}Q\left(2 + \frac{\gamma^2-1}{\gamma}Q\right)} \tag{9}$$

For this validation, the reference length is chosen as the half reaction length of the ZND profile $L_{1/2}$ i.e., the distance between the shock wave and the point where $Z = 1/2$. The ZND profile is used as initial condition. The parameters used for the one-dimensional detonation are the overdrive factor $f = 1.0$, the heat release $Q = 50$, the activation energy $E = 20$, and the specific heat ratio $\gamma = 1.2$. These parameters resulted in a detonation Mach number of 6.216. Two different mesh resolutions were employed and they ensued in 8 and 16 points per half-reaction length respectively. The boundary condition imposed is zero-order flux condition. The initial pressure is 1.0. The pressure profiles of the one-dimensional detonation wave propagation for the case with 8 points per half reaction length and 16 points per half reaction length are shown in Figs. 2 and 3 respectively. The results indicate a satisfactory convergence of the WENO solver. The results also corroborate with the published material by Dou et al.[6] Hence, the chemical reaction solver was verified by simulating the propagation of a detonation wave in one dimension.

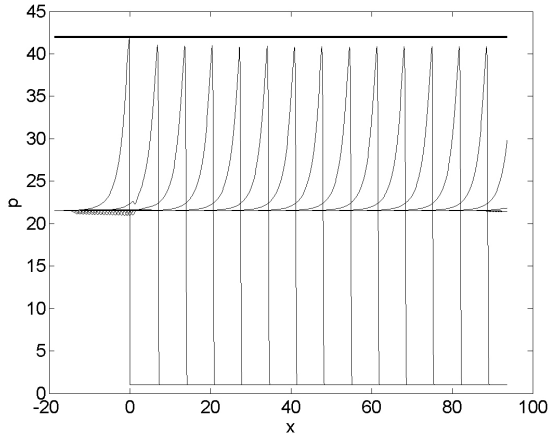

Figure 2. One-dimensional detonation wave simulated by using the 5^{th}-order WENO scheme with $dx = L_{1/2}/8$; wave propagating from left to right.

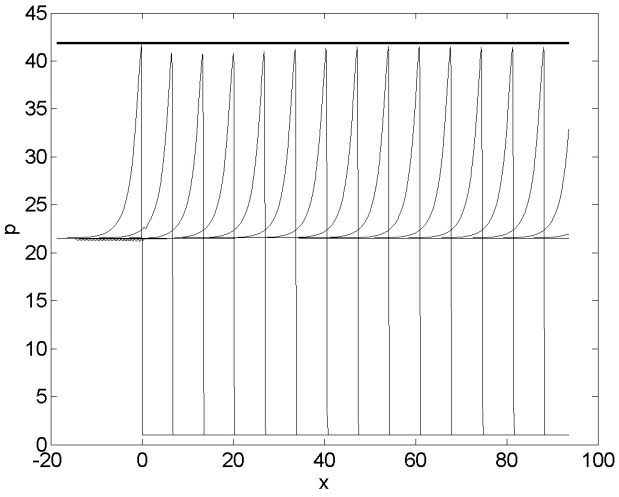

Figure 3. One-dimensional detonation wave simulated by using the 5^{th}-order WENO scheme with $dx = L_{1/2}/16$; wave propagating from left to right.

III.C. Validation of the Three-Dimensional WENO Euler Code

The three-dimensional WENO Euler code was used to capture the physics of a moving shock wave at Mach 3 interacting with a sinusoidal density variation. The computational domain is $[-5, 5]$ and the simulation was carried out with two different grid resolutions, namely, $\{N_1,\ N_2,\ N_3\} = \{50,\ 5,\ 5\}$ and $\{200,\ 5,\ 5\}$ where $\{N_1,\ N_2,\ N_3\}$ are the number of grid points in x, y, z directions respectively. Zero-order boundary conditions are employed in all the three directions and dimension-by-dimension reconstruction is adopted. The initial conditions used are given by

$$(\rho, u, P) = \begin{cases} 3.85714, 2.6294, 10.3333 & x < -4 \\ 1 + \epsilon \sin 5x, 0, 1 & x >= -4 \end{cases}$$

Here, $\epsilon = 0.2$. The computed density is plotted for two different times, say, $t = 1.0$ and 1.8.

Results pertaining to the resolution of $200 \times 5 \times 5$ are shown in Fig. 4. These trends corroborate the published results for the 5^{th}-order WENO scheme.[18] It is clear that the 5^{th}-order WENO scheme resolves the salient features of the flow accurately.

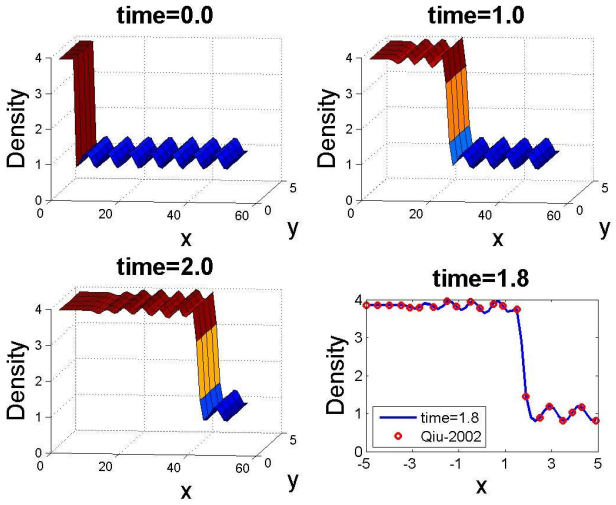

Figure 4. The shock–density wave interaction problem; visualizing the three-dimensional data in two dimension along a slice in z. Bottom right graph is one-dimensional visualization of the three-dimensional data. Wave propagating from left to right.

III.D. Validation of the Three-Dimensional WENO Navier–Stokes Code

The three-dimensional Euler code was converted to a Navier–Stokes code by considering the viscous terms. The code was validated by two different problems, viz., simulation of the decay of compressible homogeneous isotropic turbulence (CHIT) and simulation of the interaction of a shock wave and CHIT.

DNS of Compressible Homogeneous Isotropic Turbulence

Turbulence has been examined experimentally, analytically and numerically for many decades.[42–51] Relevance of theoretical methods on homogeneous isotropic turbulence flow investigation is discussed by several authors.[45,52–56] Experimental evidence on turbulence energy spectra revealed that all spectra collapse to a universal curve.[46] Different facets of compressible turbulence are reviewed by Lele.[44] Direct numerical simulation of decay of isotropic turbulence using 64^3, 128^3 and 256^3 resolution shows good agreement with experimental results, see Mansour.[57,58] The simulations also revealed that nonlinear terms play a vital role in energy evolution even at low Reynolds number. Statistics of the spatial evolution of turbulence such

as turbulence intensity, vorticity, and velocity derivative skewness show that they are identical to results obtained from temporal evolution via Taylor's hypothesis except dilatation term, see Lee.[59] Limitations of the Taylor's hypothesis are discussed by Lee et al.[1] Conditions for the occurrence of eddy shocklets in compressible turbulence decay were examined by Lee.[60] Three-dimensional turbulence is found to be less sensitive to the initial compressibility, and requires higher initial M_t for eddy shocklets to form than for two-dimensional turbulence. It was also found that higher M_t and higher Re increase the probability of occurrence of eddy shocklets.

The effect of compressibility on the dynamics and structures on turbulence decay are examined by Pirozzoli and Grasso.[61] This study revealed that the joint probability density function has a universal structure. Even for compressible turbulence, the growth of enstrophy is associated to a preferential alignment of the vorticity with the intermediate eigenvector of the anisotropic part of the strain-rate tensor as for incompressible turbulence. Pressure–dilatation correlation and its significance were analyzed by Sarkar.[62] Compressibility tends to reduce spatial intermittency in fully-developed turbulence, see Shivamoggi.[63] The energy decay in physical space is traced using the Lagrangian correlation coefficient between local kinetic energy at different scales, see Meneveau et al.[64] The Kolmogorov energy cascade is expected to be little affected by compressibility, and therefore remains independent of rms Mach number (M_t).[65] On the analysis of DNS data of compressible turbulence decay using the Helmholtz decomposition of the velocity field, Miura et al.[66] found that the pressure–dilatation term yields a dominant contribution to the exchange of compressive kinetic energy and internal energy.

Thermodynamic analysis of DNS data revealed that lower initial turbulent Mach number results in simple thermodynamics scalings whereas higher turbulent Mach number result in more complex thermodynamic scalings.[67] Analysis of the rate of strain tensor in compressible homogeneous turbulence helped to deduce the presence of structures. Moreover, their shapes and orientations are quite different from those found in incompressible flows.[68] The results also confirmed that the vorticity and the dilatation are uncorrelated and statistically independent. The investigation by Goto[69] on the physical mechanism for energy cascade is found to be due to the stretching of smaller scale vortices by tubular vortex pairs. Vortex extraction studies were discussed by using wavelet decomposition,[70] by using curvelet transform[71] and by using DNS.[72]

Porter[48] performed the simulation of decaying compressible turbulence with grid resolution of 512^3 and 1024^3 which revealed that the flow exhibits a self-similar character in long-range wavenumbers. DNS of incompressible turbulence based on the Fourier spectral method is carried out with 4096^3 grid resolution by Ishihara et al.[73,74]

The simulation of weakly compressible homogeneous isotropic decaying turbulence is carried out to validate the solver. The initial energy spectrum is the Mansour–Wray spectrum[57]

$$E(k,0) = \frac{q^2}{2A}\frac{1}{k_p^{\sigma+1}k^{\sigma}}\exp\left[-\frac{\sigma}{2}\left(\frac{k}{k_p}\right)^2\right] \tag{10}$$

where k_p is the wave number at which $E(k, 0)$ is maximum, σ is a parameter, and

$$A = \int k^{\sigma}\exp\left(-\frac{\sigma k^2}{2}\right)dk \tag{11}$$

The energy spectrum is related to the amplitude of the Fourier modes of the velocity components and also provides random and isotropic field. This particular energy spectrum is chosen because it has proved itself to represent low and moderate Reynolds number turbulent flow with a good match to experimental data.[57] The velocity components are generated by three sets of random numbers that permit the uniform distribution of the angles (θ_1, θ_2, ϕ) on the interval (0, 2π). The velocity components are

$$\tilde{u}_1 = \frac{\alpha|k|k_2 + \beta k_1 k_3}{|k|k_h} \tag{12a}$$

$$\tilde{u}_2 = \frac{-\alpha|k|k_2 + \beta k_3 k_2}{|k|k_h} \tag{12b}$$

$$\tilde{u}_3 = \frac{\beta k_h^2}{|k|k_h}. \tag{12c}$$

The tilde symbol indicates that these are complex quantities. The above expressions fulfill the requirement of a solenoidal velocity field in wave-number space, namely, $k_i u_i = 0$. Moreover, it can be shown that if

$$\alpha = \frac{E(k,0)}{4\pi k^2} \exp(l\theta_1) \cos(\phi) \tag{13a}$$

$$\beta = \frac{E(k,0)}{4\pi k^2} \exp(l\theta_2) \cos(\phi) \tag{13b}$$

the three-dimensional energy spectrum of this field is equal to $E(k, 0)$. These initial conditions were used by Rogallo.[42]

The high time and length scale resolution for turbulence and chemical reaction mandates parallelism for the code. The three-dimensional compressible Navier–Stokes code with WENO solver is parallelized using message passing interface (MPI). Each MPI process is in charge of a piece of the three-dimensional domain. All MPI processes have the same number of grid points and the same computational load. Inter-processor communication is only between nearest neighbors in a three-dimensional topology.

Simulation of the temporal decay of weakly compressible homogeneous isotropic turbulence was carried out using four different grid resolutions (32^3, 64^3, 128^3, 256^3). The computational domain is $[2\pi \times 2\pi \times 2\pi]$. The simulation was carried out using uniform grid spacing in all the three directions. Periodic boundary conditions were employed in the three directions and dimension-by-dimension reconstruction was adopted. The density, turbulent Mach number, pressure and the Reynolds number based on the Taylor length scale governed the generation of the initial turbulent field. Initialization of isotropic turbulence began with uniform density and pressure, but with completely random velocity values.

Validation of the 5^{th}-order WENO scheme for turbulence simulation was accomplished by comparing the DNS results of an incompressible turbulence simulation based on the Arakawa solver and the DNS results of weakly compressible turbulence obtained using the WENO scheme. It must be noted that the incompressible turbulence simulation based on Arakawa solver was already validated against the experimental data of Comte-Bellot & Corsin (1971) at $Re_\lambda = 60.7$ and that of Mansour & Wray (1994) at $Re_\lambda = 56.2$. In both cases, all the parameters were maintained identical and were compared with 64^3 grid resolution. In the compressible homogeneous turbulence simulation, the initial turbulent Mach number was 0.282, the isentropic index was 1.4, the Lewis number was 1.0 and the Prandtl number was 0.72. The Reynolds number was 1000 in both the CHIT and incompressible HIT simulation.

The rms values of the velocities in the three directions matched closely with those obtained using the incompressible turbulence code. The results are shown in Fig. 5, where vrms(1), vrms(2), vrms(3) refer to the rms of velocities in the (x, y, z) directions respectively and prms is the rms of the pressure. Also, shown is the agreement of the turbulent statistical parameters of weakly compressible turbulence and incompressible turbulence simulation.

Comparison of the total energy spectrum in Kolmogorov scales at $Re_\lambda = 32$ of both incompressible turbulence and weakly compressible turbulence is shown in Fig. 6(a). Figure 6(b) also shows the comparison of energy spectra in Kolmogorov scale at $Re_\lambda = 55$ and 32 of all the three grid resolutions. Figure 6(b) also compares the present weakly compressible turbulence results with experimental data of Compte-Bellot & Corrsin ($Re_\lambda = 60.7$) and numerical simulations of Mansour & Wray ($Re_\lambda = 56.2$), and Orlandi ($Re_\lambda = 54.3$), that is, at almost similar values of Re_λ. This figure shows that data for grids of 128^3 and above result in a trend which matched closely with the experimental data of Compte-Bellot & Corrsin and other numerical simulations. The $-5/3$ decay is also evident as indicated in the figure.

Turbulence statistics such as dissipation rate, Reynolds number based on the Taylor length scale, Taylor length scale and Kolmogorov length scale for the three grid resolutions are illustrated in Fig. 7. It also shows the trend of energy and enstrophy decay.

Fig. 8 shows the rms of the velocity in three direction and the trend of turbulent Mach number with time of all the three grid resolution under examination. It indicates isotropy is maintained.

All of the turbulence statistics show good agreement with published numerical and experimental results. The applicability of the 5^{th}-order WENO solver to capture turbulence has been validated with earlier experimental and numerical studies.[57, 58]

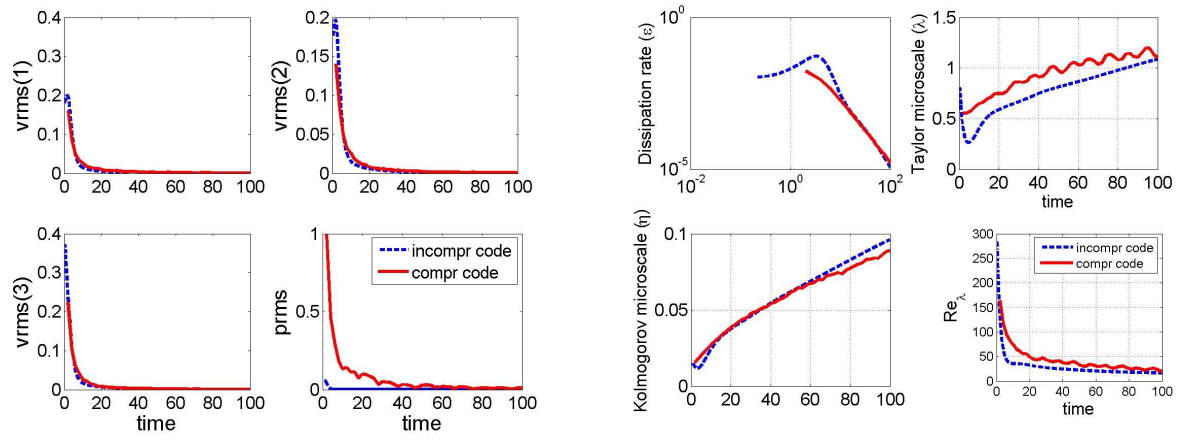

(a) (b)

Figure 5. (a) RMS of velocities and pressure (b)Turbulence statistical parameters.

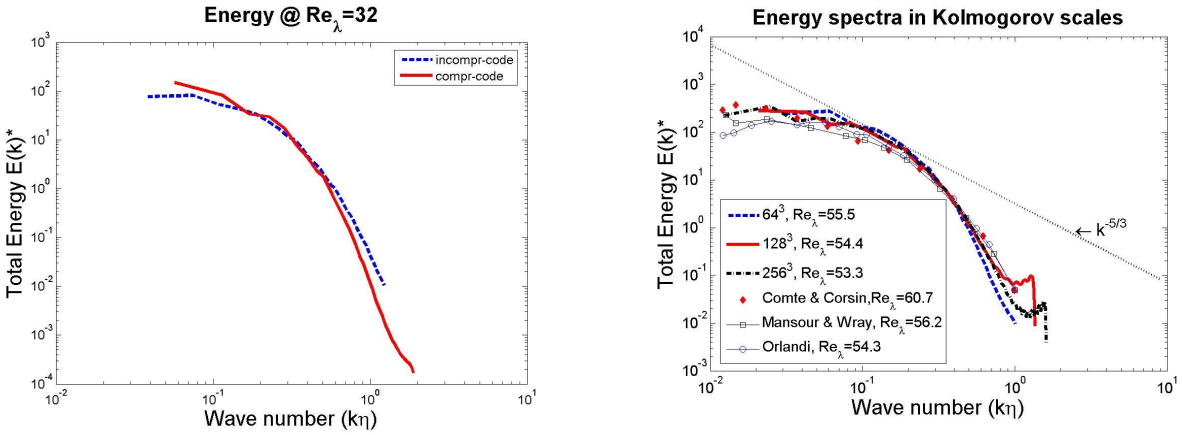

Figure 6. The energy spectra in Kolmogorov scale (a)$Re_\lambda = 32$ (b)$Re_\lambda = 55$.

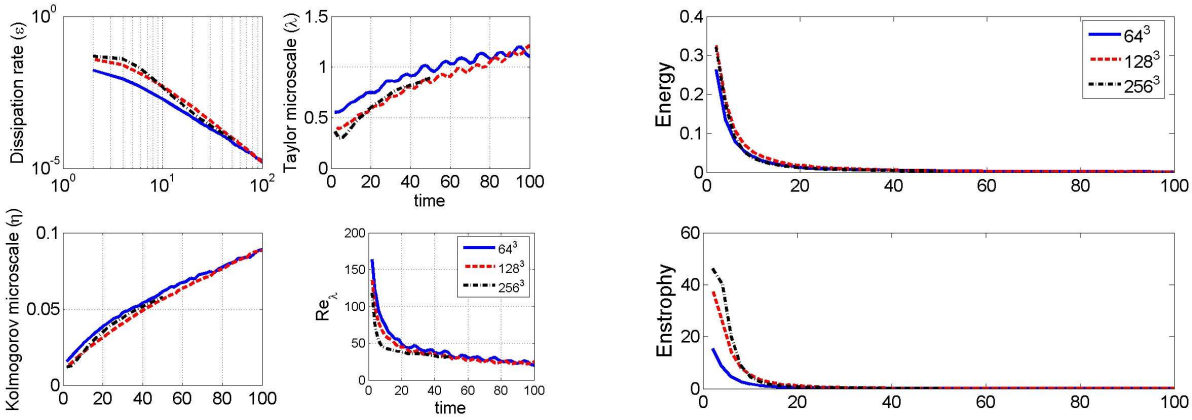

Figure 7. Trend of dissipation, energy and enstrophy with time.

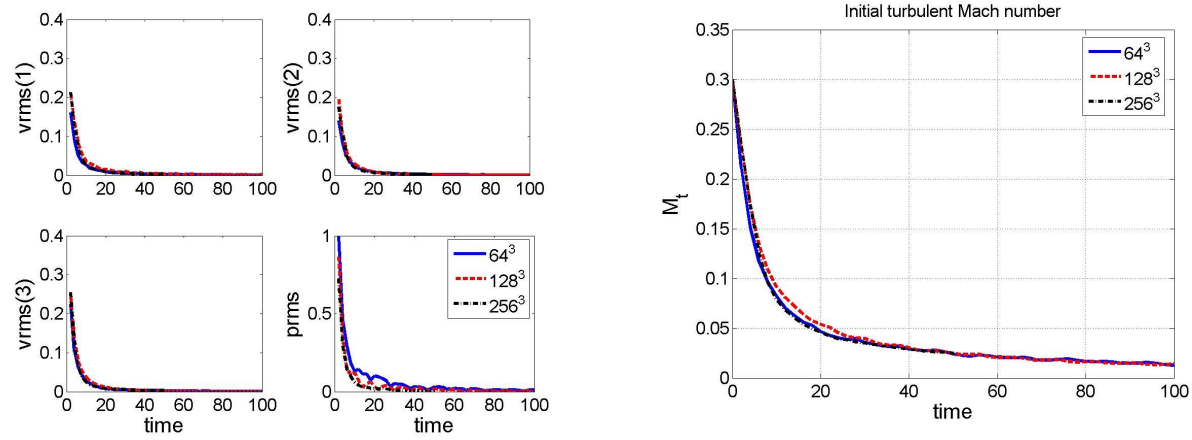

Figure 8. (a) RMS of the velocity in three directions (b)Turbulent Mach number trend

DNS of Shock Wave Interaction with CHIT

A shock wave exhibits substantial unsteadiness and deformation as a result of the interaction, whereas the characteristic velocity, timescales, length scales of turbulence change considerably. The outcome of the interaction depends on the strength, orientation, location and shape of the shock wave as well as the flow geometry and boundary conditions. Several theoretical studies have also been carried out by Ribner.[2,75] Linear interaction analysis of these interactions revealed that fluctuations amplify with length scale decrease across the shock wave. Significant acoustic noise was also found to be generated.[75] An excellent review on the physics behind shock wave and turbulence interaction is given by Andreopoulos et al.[76]

Anyiwo and Bushnell revisited the same research to understand the primary mechanisms of turbulence enhancement.[77] Numerical results also corroborated that the results of linear analysis are valid for range of parameters such as shock strength, incidence angle, amplitude of waves.[78] In the report by Jacquin et al.,[79] it was shown that rapid distortion theory was inappropriate for the analysis of shock–turbulence interaction.

Jamme et al.[80] used DNS to study the interaction between normal shock waves of moderate strength and turbulence generated using Kovasznay's decomposition. Interaction of moderately strong shock with a pre-existing turbulence showed an overall amplification of vorticity as has been noted for the case of a weak shock.[81] However, LIA indicates amplification of transverse vorticity and reduction of streamwise vorticity.

Fundamental aspects of shock–turbulence interaction and their modeling were reviewed by Lele.[44] Investigation of the effect of shock-normal Mach number on turbulence was carried out using both direct numerical simulation and linear analysis with stronger shock waves. The investigation revealed that the TKE is amplified across the shock wave and also the amplification saturates beyond $M_1 = 3.0$.[1,82] It was also observed that most turbulent length scale decrease across the shock wave while the dissipation length scale increase for $M_1 < 1.65$. Here, M_1 refers to shock Mach number. Fluctuations in thermodynamic variables are nearly isentropic for $M_1 < 1.2$ and deviate significantly from isentropy for the stronger shock waves. The energy spectrum was found to show higher energy levels at large wavenumbers, leading to an overall length scale decrease.

The interaction of the normal shock-wave with compressible HIT using DNS was carried out as the last validation for the Navier-Stokes solver. The simulation was carried out with several grid resolutions (32^3, 64^3, 128^3, 256^3).

Zero-order flux boundary conditions were imposed in the streamwise direction while periodic boundary conditions were imposed in y and z directions. The computational domain is a cube with a dimension of $(2\pi \times 2\pi \times 2\pi)$. An evenly spaced Cartesian grid discretizes this domain into N^3 points. The following four parameters govern the generation of the initial turbulent field, viz., density, turbulent Mach number, pressure, and the Reynolds number based on the Taylor length scale. Initialization of isotropic turbulence begins with uniform density and pressure, and completely random velocity values. The initial energy spectra were obtained using the Mansour–Wray energy model. The field is deemed to have reached a proper state of isotropic turbulence when the skewness of the velocity derivatives becomes the desired value observed in experimental data. Once the turbulence simulation reached the desired skewness value, a normal shock wave was allowed to propagate through the cube. The WENO scheme's ability to capture accurately the flow discontinuities is made use of in this interaction.

The length scale L is $1/k_0$, the density scale is the mean preshock value, the velocity scale is the turbulence velocity rms, and the pressure scale is the product of the density scale and velocity scale squared. The post- and pre-shock conditions in the simulation of shock-turbulence case are given below

$$p_l = \frac{u_{rms}^2 \left(2\gamma M_s^2 - \gamma + 1\right)}{\left(\gamma^2 + \gamma\right) M_t^2} \tag{14a}$$

$$\rho_l = \frac{M_s^2 \left(1 + \gamma\right)}{2 + \left(\gamma - 1\right) M_s^2} \tag{14b}$$

$$u_l = \frac{2u_{rms} \left(M_s^2 - 1\right)}{\left(1 + \gamma\right) M_s M_t} \tag{14c}$$

$$p_r = \frac{u_{rms}^2}{\gamma M_t^2} \tag{14d}$$

$$\rho_r = 1 \tag{14e}$$

$$u_r = 0 \tag{14f}$$

Figure 9 shows the energy spectra before and after the propagation of the shock wave. Interaction of the shock wave with turbulence resulted in a corrugation of the shock front (not shown for brevity). The total energy levels were raised at high wave numbers as also observed by Lele et al.[44]

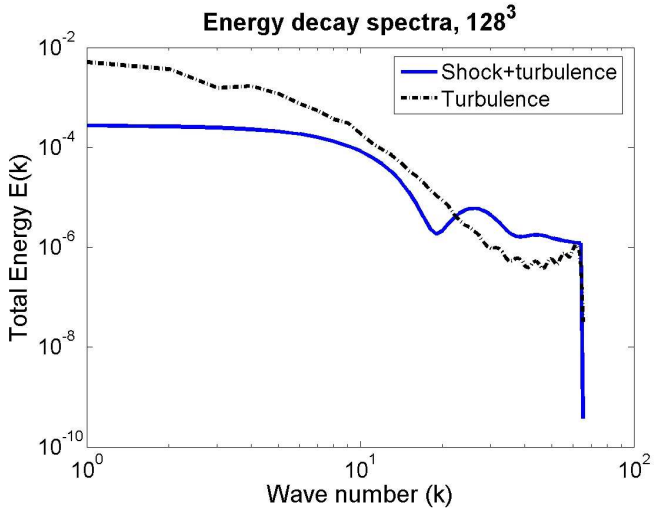

Figure 9. Comparison of energy spectra of shock+turbulence and detonation+turbulence simulations.

IV. DNS of Interaction of Detonation Wave with CHIT

Application of understandings of interaction of detonation wave and turbulence can be envisaged as hypersonic propulsion systems viz, SCRAMJET engines, pulse detonation engines, etc. Very limited research has been done in the field of the interaction of detonation wave and turbulence. Due to the complexity involved in its physics, these studies were carried out by simplifying the process using linear interaction theory and analytical methods.[3,5,83,84]

The interaction of the detonation wave with CHIT using DNS is carried out using the Navier–Stokes solver. All the numerical and initial conditions were the same as for the shock interaction case described above. Moreover, the viscous decay process was characterized by the Reynolds, Lewis and Prandtl numbers. A power law with exponent $n = 0.7$ was used for the viscosity–temperature relation. The Lewis and Prandtl numbers are independent of the fluid solution, leading to linear scaling between viscosity, thermal conductivity and diffusivity.

The length scale L is $1/k_0$, the density scale is the mean preshock value, the velocity scale is the turbulence velocity rms, and the pressure scale is the product of the density scale and velocity scale squared. The pre- and post- detonation conditions in the simulation of detonation-turbulence case are given below

$$\rho_r = 1 \tag{15a}$$

$$p_r = \rho_r \frac{u_{rms}^2}{\gamma M_t^2} \tag{15b}$$

$$u_r = -M_{Det}\sqrt{\frac{\gamma p_r}{\rho_r}} \tag{15c}$$

$$p_l = \frac{1 + \gamma M_{Det}^2 + \sqrt{\gamma\left(\gamma\left(M_{Det}^2 - 1\right)^2 - 2\left(\gamma^2 - 1\right) Y M_{Det}^2 Q\right)}}{\gamma + 1} \tag{15d}$$

$$u_l = \frac{M_{Det}\sqrt{\gamma p_l}\left(\gamma\left(2 + \left(\gamma - 1\right) M_{Det}^2\right) + 2\left(\gamma - 1\right) Y Q\right)}{\gamma + \gamma^2 M_{Det}^2 + \sqrt{\gamma\left(\gamma\left(M_{Det}^2 - 1\right)^2 - 2\left(\gamma^2 - 1\right) Y M_{Det}^2 Q\right)}} \tag{15e}$$

$$\rho_l = \rho_r \frac{u_r - w_s}{u_l - w_s} \tag{15f}$$

IV.A. Results

The study was carried out with three values of the non-dimensional heat release Q, three values of the non-dimensional activation energy E and with two different grid resolutions as shown in Table 1. The two parameters of greatest interest are the turbulent Mach number M_t and a new non-dimensional number N which represents the ratio of turbulence length scale to reaction scale. These parameters establish a relationship in the characteristic lengths and times between the two fundamental processes, viz., the detonation and the turbulence. The viscous decay is in fact too slow to contribute to the interaction; thus the Reynolds, Lewis and Prandtl numbers are fixed. The influence of other parameters Q, E, f, k_p, σ will also be considered. The number of points in the half-reaction length was maintained as 12. The other input parameters were $f = 1.2$, $k_p = 3$, $\sigma = 4$, $Pr = 0.72$, $Re = 1000$, $Le = 1$, $N = 1$ and $\gamma = 1.2$. The skewness of the velocity derivative in the three directions pre-detonation were -0.48, -0.51 and -0.49 respectively for the 128^3 grid resolution case.

Table 1. The initial condition of the numerical simulations.

Case	N_x	N_y	N_z	M_t	Re_λ	E	Q	M_{Det}
1	32	32	32	0.0534	25.72	10	10	3.327
2	32	32	32	0.0534	25.72	17	17	4.156
3	32	32	32	0.0534	25.72	20	20	4.464
4	128	128	128	0.064	49.35	10	10	3.327
5	128	128	128	0.064	49.35	17	17	4.156
6	128	128	128	0.064	49.35	20	20	4.464

Figure 10 shows the variation of the turbulent Mach number with the non-dimensional time for both shock–turbulence and detonation–turbulence interactions. The shock–turbulence interaction was evaluated with a freestream Mach number identical to that of the detonation analysis, $M_0 = 4.156$. The figure also compares the post-interaction total energy spectra. The results reveal that the detonation–turbulence interaction shows more amplification in the energy in the moderate to high wave number range whereas the shock–turbulence interaction shows amplification in the high wave number range only.

The effect of heat release and activation energy on the statistical parameters of the turbulence and energy are examined. Figure 11 illustrates that the heat release leads to an increased level of fluctuation in the post shock region. The right side of the figure shows that the rms values of the velocity and pressure go hand-in-hand with the heat release. The rms velocity in the streamwise direction is initially $O(1000)$ higher than those in the transverse directions immediately after the wave passage. However, the rms values decrease rapidly and reaches values comparable to the transverse directions when $t > 0.5$. It must be noted that the amplification of the rms of the velocity in the streamwise direction is considerably higher than the amplification of the rms of the velocities in the transverse directions.

The detonation–turbulence interaction resulted in a sharp drop in vorticity fluctuation initially and which then rose moderately until the resumption of the turbulence decay. Increasing the heat release speeded up the rise and fall of vorticity decay trend, see Fig. 12. The right side of the figure indicates the change in the Reynolds stresses due to detonation–turbulence interaction. The variation in heat release did not have much

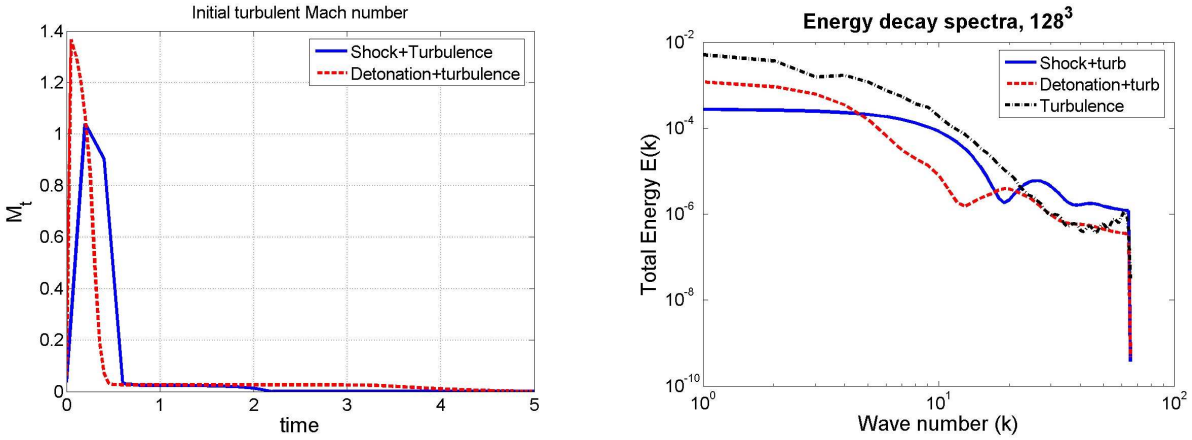

Figure 10. Comparison of shock–turbulence and detonation–turbulence interaction.

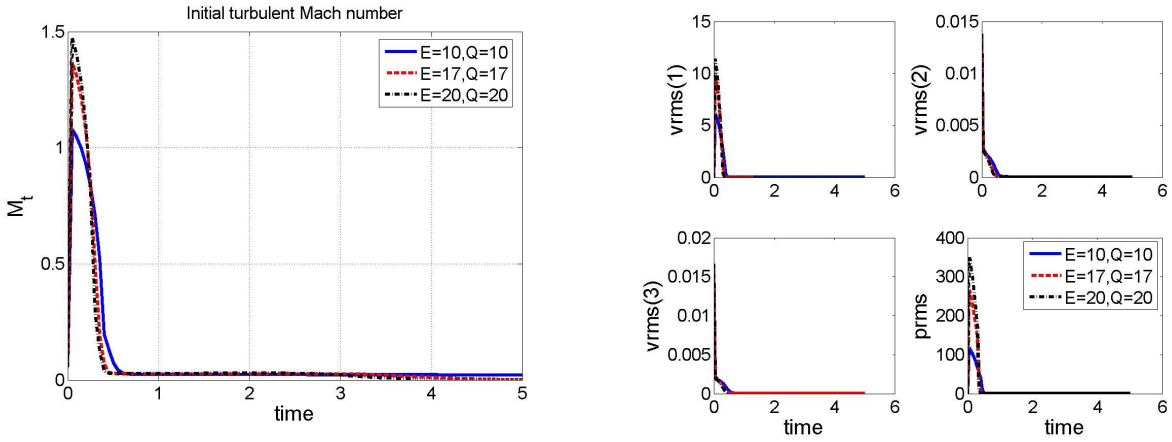

Figure 11. Effect of heat release on turbulent Mach number and rms of velocities and pressure.

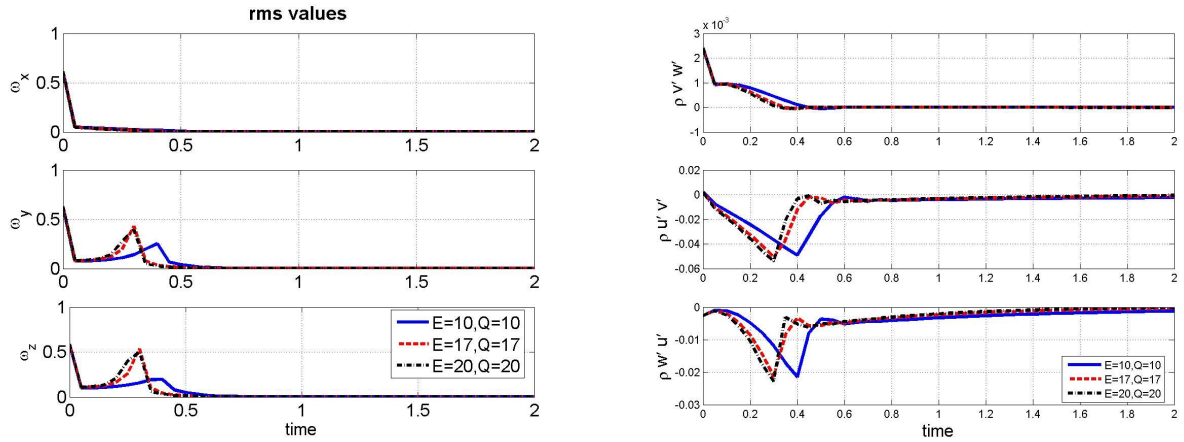

Figure 12. Effect of heat release on rms of vorticity and Reynolds stresses.

effect on the trend of Reynolds stresses with time. The variation of heat release and activation energy resulted in higher amplification of thermodynamic parameters, see Fig. 13. The right-side subfigures indicate that the detonation–turbulence interaction also resulted in an increase in turbulence length scales (Kolmogorov length scale and Taylor microscale). The higher the heat release, the greater is the length scale increase. Further, the drastic drop in dissipation rate indicates that there is a drastic drop in turbulent kinetic energy due to the detonation–turbulence interaction. There is an increase in the dissipation of turbulent kinetic energy with increase in heat release parameter. The Reynolds number based on the Taylor microscale is higher for higher heat release and there is a faster decline in Re_λ with an increase in the heat release parameter.

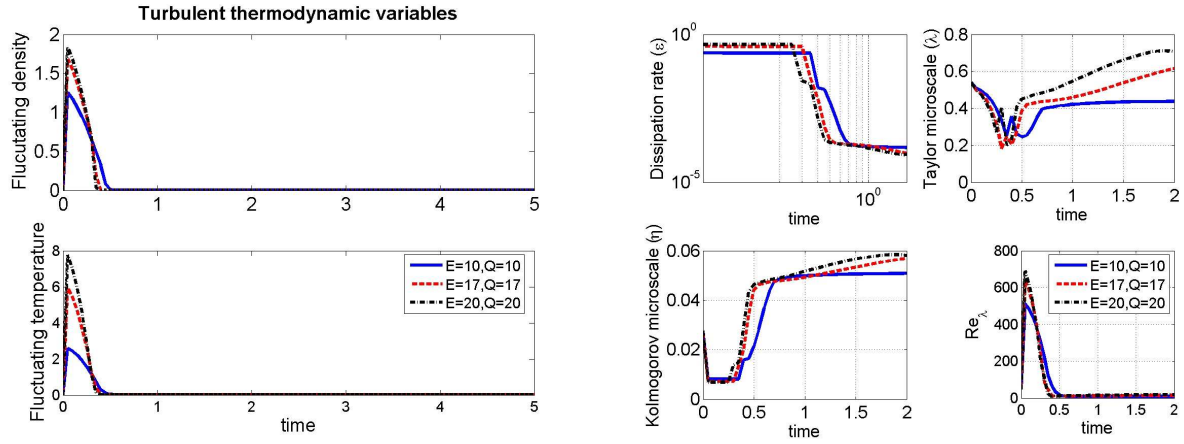

Figure 13. Effect of heat release on rms of thermodynamic parameters and turbulence statistics.

The post-detonation total energy spectrum for the turbulence–detonation interaction is shown in Fig. 14. The left subfigure corresponds to the post-detonation spectrum obtained at $t = 1$. It indicates that the energy at high wave numbers is inversely proportional to the heat release. The total energy spectrum plot obtained at $t = 5$ indicates that the energy decay is faster in the highest energy release whereas it is slower in the lowest heat release. It also showed rapid cascade of energy to small scales.

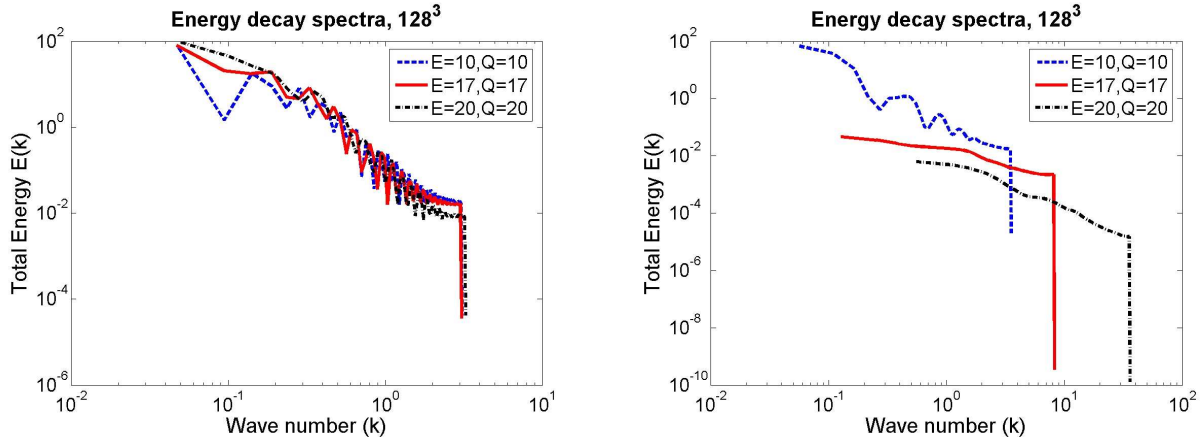

Figure 14. Effect of heat release on energy spectra, time = 1 (left) and time = 5 (right).

V. Conclusions

In summary, the detonation wave and turbulence interaction resulted in the following observations

1. The detonation wave becomes corrugated.
2. The interaction resulted in higher energy at higher wave numbers in the moderate to low scales whereas the shock-turbulence resulted in higher energy at small scales only.
3. There is a rapid energy decay, with the decay being more rapid with higher heat release.
4. The higher the heat release, the higher the amplification of the rms of velocities, turbulent Mach number and thermodynamic parameters.
5. The detonation–turbulence interaction resulted in much higher increase in turbulence length scale than that was observed in shock–turbulence interaction case and also the increase in length scales was directly proportional to the heat release.
6. Rapid cascade of energy to small scales was observed in the post detonation wave energy spectrum.

VI. Acknowledgments

The authors expresses our sincere thanks to the Texas Advanced Computing Center for the high performance computation and visualization support. The first author also thank Dr. Randall Leveque for his valuable help on the WENOCLAW package.

References

[1]Lee, S., Lele, S. K., and Moin, P., "Interaction of isotropic turbulence with shock waves: effect of shock strength." *Journal of Fluid Mechanics*, Vol. 340, 1997, pp. 225–247.

[2]Ribner, H. S., "Spectra of noise and amplified turbulence emanating from shock-turbulence interaction," *AIAA*, Vol. 25, 1987, pp. 436–442.

[3]Massa, L. and Lu, F. K., "Role of the induction zone on turbulence-detonation interaction," *Physics of Fluids*, Vol. 0, 2008, pp. 0.

[4]Powers, J. M., "Review of multiscale modeling of detonation," *Journal of Propulsion and Power*, Vol. 22, 2006, pp. 1217–1229.

[5]Jackson, T. L., Hussaini, M. Y., and Ribner, H. S., "Interaction of turbulence with a detonation wave," *Physics of Fluids*, Vol. 5, 1993, pp. 745–749.

[6]Dou, H. S., Tsai, H. M., Khoo, B. C., and Qiu, J., "Simulations of detonation wave propagation in rectangular ducts using a three-dimensional WENO scheme," *Combustion and Flame*, Vol. 154, 2008, pp. 644–659.

[7]Deledicque, V., *Modeling and simulation of multidimensional compressible flows of gaseous and heterogeneous reactive mixtures*, Ph.D. thesis, Universite catholique de Louvain, 2007.

[8]Leveque, R. J., "WENOCLAW," 2006.

[9]Titarev, V. A. and Toro, E. F., "Finite volume WENO schemes for three-dimensional conservation laws," *Jou. of Computational Physics*, Vol. 201, 2004, pp. 238–260.

[10]Shu, C. W., "Essentially Non oscillatory and Weighted essentially non oscillatory schemes for hyperbolic conservation laws," *NASA CR 97 206253*, 1997, pp. 1–78.

[11]dong Liu, X., Osher, S., and Chan, T., "Weighted essentially non-oscillatory scheme," *Jou. of Computational Physics*, Vol. 115, 1994, pp. 200–212.

[12]Henrick, A. K., Aslam, T. D., and Powers, J. M., "Mapped weighted essentially non-osciallatory schemes Achieving optimal order near critical points," *Physics of Fluids*, Vol. 207, 2005, pp. 542–567.

[13]Shi, J., Hu, C., and Shu, C. W., "A technique of treating negative weights in WENO schemes," *Jou. of Computational Physics*, Vol. 175, 2002, pp. 108–127.

[14]Levy, D., Puppo, G., and Russo, G., "Central WENO schemes for hyperbolic systems of conservation laws," *Mathematical modelling and Numerical Analysis*, Vol. 33, 1999, pp. 547–571.

[15]Balsara, D. S. and Shu, C. W., "Monotonicity preserving weighted essentially non oscillatory schemes with increasingly high order accuracy," *Jou. of Computational Physics*, Vol. 160, 2000, pp. 405–452.

[16]Hu, C. and Shu, C. W., "Weighted essentially non oscillatory schemes on triangular meshes," *Journal of Computational Physics*, Vol. 150, 1999, pp. 97–127.

[17]Serna, S. and Marquina, A., "Power ENO methods a fifth order accurate Weighted Power ENO method," *Journal of Computational Physics*, Vol. 194, 2003, pp. 632–658.

[18]Qiu, J. and Shu, C. W., "On the construction comparison and local characteristic decomposition for higher order central WENO schemes," *Journal of Computational Physics*, Vol. 183, 2002, pp. 187–209.

[19]Taylor, E. M., Wu, M., and Martin, M. P., "Optimisation of nonlinear error for weighted essentially non-osciallatory methods in direct numerical simulations of compresssible turbulence," *Jou. of Computational Physics*, Vol. 223, 2007, pp. 384–397.

[20]Jiang, G. and Shu, C., "Efficient implementation of weighted ENO schemes," *Journal of Computational Physics*, Vol. 126, 1996, pp. 202–228.

[21]White, D. R., "Structure of gaseous detonation III density in the induction region of hydrogen detonation," *Physics of Fluids*, Vol. 6, 1963, pp. 1011–1015.

[22]Kailasanath, K., "Review of propulsion applications of detonation waves," *AIAA*, Vol. 38, 2000, pp. 1698–1708.

[23]Hanana, M., Lefebvre, M. H., and Tiggelen, P. J. V., "Preliminary experimental investigation of the pressure evolution in detonation cells," *Experimental thermal and Fluid science*, Vol. 21, 2000, pp. 64–70.

[24]Hoke, J., Bradley, R., and Schauer, F., "Heat transfer and thermal management in a pulsed detonation engine," *AIAA 6486*, 2003.

[25]X.Y. Hu, D.L. Zhang, Z. J., "Analytical study of idealized two-dimensional cellular detonations," *Shock Waves Springer Verlag 2002*, Vol. 11, 2002, pp. 475–480.

[26]Li, J., Lai, W. H., Chung, K., and Lu, F. K., "Experimental study on transmission of an overdriven detonation wave from propane oxygen to propane air," *Combustion and Flame*, Vol. 1.91, 2008, pp. 1–15.

[27]Panicker, P. K., Lu, F. K., and Wilson, D. R., "Practical issues in ground testing of pulsed detonation engines," *IMECE 44068*, 2007.

[28]Bazhenova, T. V. and Golub, V. V., "Use of gas detonation in a controlled frequency mode review," *Combustion, Explosion and Shock Waves*, Vol. 39, 2003, pp. 365–381.

[29]Hu, X. Y., Czerwinska, J., Adams, N., and Khoo, B. C., "The cellular structure and its tracks of a H_2 O_2 Ar detonation waves," *ICATM*, Vol. 21, 2004, pp. 15–21.

[30]Oran, E. S. and Boris, J. P., "Numerical Approaches to Combustion Modeling," *AIAA (Progress in Astronautics and Aeronautics)*, Vol. 135, 1991.

[31]Oran, E. S. and Boris, J. P., *Numerical Simulation of Reactive Flow*, Elsevier Science Publishing Company, Newyork USA, 1991.

[32]Gamezo, V. N., Khokhlov, A. M., and Oran, E. S., "Deflagrations and Detonations in Thermonuclear Supernovae," *Phy. Review Letters*, Vol. 92, 2004, pp. 1–4.

[33]Gamezo, V. N., Desbordes, D., and Oran, E. S., "Two-dimensional reactive flow dynamics in cellular detonation waves," *Shockwaves*, Vol. 9, 1999, pp. 11–17.

[34]Tsuboi, N., Daimon, Y., and Hayashi, A. K., "Three-dimensional numerical simulation of detonations in coaxial tubes," *Shockwaves*, Vol. 18, 2008, pp. 379–392.

[35]Eto, K., Tsuboi, N., and Hayashi, A. K., "Numerical study on three-dimensional C-J detonation waves detailed propagating mechanism and existence of OH radical," *Proceedings of the Combustion Institute*, Vol. 30, 2005, pp. 1907–1913.

[36]Helzel, C., *Numerical approximation of conservation laws with stiff source term for the modeling of detonation waves*, Ph.D. thesis, der Otto-von-Guericke-Universitat Magdeburg, 2000.

[37]Leveque, R. J., "Some traffic flow models illustrating interesting hyperbolic behaviour," *SIAM Annual meeting and minisymposium*, Vol. 0, 2001, pp. 11.

[38]Akkerman, V., Bychkov, V., Petchenko, A., and Eriksson, L.-E., "Accelerating flames in cylindrical tubes with nonslip at the walls," *Combustion and Flame*, Vol. 145, 2006, pp. 206–219.

[39]He, H., *Numerical simulations of unsteady flows in a pulse detonation engine by the space time conservation element and solution element method*, Ph.D. thesis, The Ohio State University, 2006.

[40]Kuo, K. K., *Principles of combustion*, John Wiley and Sons, New Jersey, USA, 2005.

[41]Fickett, W. and Davis, W. C., *Detonation Theory and Experiment*, Dover Publications, Mineola NY 11501, 1969.

[42]Rogallo, R. S., "Numerical experiments in homogeneouos turbulence," *NASA TM-81315*, 1981, pp. 1–91.

[43]Rogallo, R. S., "An ILLIAC program for the numerical simulation of homogeneous incompressible turbulence," *NASA TM 73203*, 1977, pp. 34.

[44]Lele, S. K., "Compressibility effects on turbulence," *Annu. Rev. Fluid Mech.*, Vol. 26, 1994, pp. 211–254.

[45]Moriconi, L. and Rosa, R., "Theoretical aspects of homogenous isotropic turbulence," *J. of the Braz. Soc. of Mech. Sci. and Eng.*, Vol. XXVI, 2004, pp. 391–399.

[46]She, Z. S. and Jackson, E., "On the universal form of energy spectra in fully developed turbulence," *Physics of Fluids A*, Vol. 5, 1993, pp. 1526–1528.

[47]Chassaing, P., "The modeling of variable density turbulent flows," *Flow, Turbulence and Combustion*, Vol. 66, 2001, pp. 293–332.

[48]Porter, D. H. and Woodward, P. R., "Inertial range structures in decaying compressible turbulent flows," *Physics of Fluids*, Vol. 10, 1998, pp. 237–245.

[49]Cerutti, S., Meneveau, C., and Knio, O. M., "Spectral and hyper eddy viscosity in high-Reynolds number turbulence," *Jou. Fluid Mech.*, Vol. 421, 2000, pp. 307–338.

[50]Vreman, A. W., *Direct and large eddy simulation of the compressible turbulent mixing layer*, Ph.D. thesis, de Universiteit Twente, 1995.

[51]Neda, M., *Numerical analysis and phenomenology of homogeneous isotropic turbulence generated by higher order models of turbulence*, Ph.D. thesis, University of Pittsburg, 2007.

[52]Pope, S. B., *Turbulent flows*, Cambridge University Press, Newyork, USA, 2000.

[53]Frisch, U., *Turbulence*, Cambridge University Press, Cambridge USA, 1995.

[54]Hinze, J. O., *Turbulence*, Mc-Graw-Hill, Newyork USA, 1975.

[55]Batchelor, G. K., *The theory of homogeneous turbulence*, Cambridge University Press, Cambridge USA, 1953.

[56]Bataille, F. and Zhou, Y., "Nature of the energy transfer process in compressible turbulence," *The American Physical Society*, Vol. 59, 1999, pp. 5417–5426.

[57]Mansour, N. N. and Wray, A. A., "Decay of isotropic turbulence at low Reynolds number," *Physics of Fluids*, Vol. 6, 1994, pp. 808–814.

[58]Orlandi, P., *Fluid flow phenomena*, Kluwer Academic Publishers, Netherlands, 2001.

[59]Lee, S., Lele, S. K., and Moin, P., "Simulation of spatially evolving turbulence and the applicability of Taylor's hypothesis in compressible flow," *Physics of Fluids A*, Vol. 4, 1992, pp. 1521–1530.

[60]Lee, S., Lele, S. K., and Moin, P., "Eddy shocklets in decaying compressible turbulence," *Physics of Fluids A*, Vol. 3, 1991, pp. 657–664.

[61]Pirozzoli, S. and Grasso, F., "Direct numerical simulations of isotropic compressible turbulence Influence of compressibility on dynamics and structures," *Physics of Fluids*, Vol. 16, 2004, pp. 4386–4407.

[62]Sarkar, S., "The pressure dilatation correlation in compressible flows," *Physics of Fluids A*, Vol. 4, 1992, pp. 2674–2682.

[63]Shivamoggi, B. K., "Multifractal aspects of the scaling laws in fully developed compressible turbulence," *Annals of Physics*, Vol. 243, 1995, pp. 169–176.

[64]Meneveau, C. and Lund, T. S., "On the Lagrangian nature of the turbulence energy cascade," *Physics of Fluids*, Vol. 6, 1994, pp. 2820–2825.

[65]Zeman, O., "On the decay of compressible isotropic turbulence," *Phys. Fluids A*, Vol. 3, 1991, pp. 951–955.

[66]Miura, H. and Kida, S., "Acoustic energy exchange in compressible turbulence," *Physics of Fluids*, Vol. 7, 1995, pp. 1732–1742.

[67]Cai, X. D., O'Brien, E. E., and Ladeinde, F., "Thermodynamic behaviour in decaying, compressible turbulence with initally dominant temperature fluctuations." *Physics of Fluids*, Vol. 9, 1997, pp. 1754–1763.

[68]Erlebacher, G. and Sarkar, S., "Statistical analysis of the rate of strain tensor in compressible homogeneous turbulence," *Physics of Fluids*, Vol. 5, 1993, pp. 3240–3254.

[69]Goto, S., "A physical mechanism of the energy cascade in homogeneous isotropic turbulence," *Jou. Fluid Mechanics*, Vol. 605, 2008, pp. 355–366.

[70]Roussel, O., Schneider, K., and Farge, M., "Coherent vortex extraction in 3D homogeneous turbulence comparison between orthogonal and biorthogonal wavelet decompositions," *Journal of Turbulence*, Vol. 6, 2005, pp. 1–15.

[71]Ma, J. and Hussaini, M. Y., "Three dimensional curvelets for coherent vortex analysis of turbulence," *Applied Physics Letters 184101*, Vol. 91, 2007, pp. 1–3.

[72]Miura, H., "Analysis of vortex structures in compressible isotropic turbulence," *Computer Physics Communications*, Vol. 147, 2002, pp. 552–555.

[73]Ishihara, T., Kaneda, Y., Yokokawa, M., Itakura, K., and Uno, A., "Small-Scale Statistics in High-Resolution Direct Numerical Simulation of Turbulence," *Jou. of Fluid Mechanics*, Vol. 592, 2007, pp. 335–366.

[74]Yokokawa, M., Itakura, K., Uno, A., Ishihara, T., and Kaneda, Y., "16.4-Tflops Direct Numerical Simulation of Turbulence by a Fourier Spectral Method on the Earth Simulator," *IEEE*, 2002, pp. 1–17.

[75]Ribner, H. S., "Shock-turbulence interaction and the generation of noise," *NACA*, Vol. Report 1233, 1955, pp. 19.

[76]Andreopoulos, Y., Agui, J. H., and Briassulis, G., "Shock wave turbulence interactions," *Ann. Rev. Fluid Mech.*, Vol. 32, 2000, pp. 309–345.

[77]Anyiwo, J. C. and Bushnell, D., "Turbulence amplification in shock-wave boundary layer interaction," *AIAA*, Vol. 20, 1982, pp. 893–899.

[78]Zang, T. A., Hussaini, M. Y., and Bushnell, D. M., "Numerical computations of turbulence amplification in shock-wave interactions," *AIAA*, Vol. 22, 1984, pp. 13–21.

[79]Jacquin, L., Cambon, C., and Blin, E., "Turbulence amplification by a shockwave and rapid distortion theory," *Physics Fluids A*, Vol. 5, 1993, pp. 2539–2550.

[80]Jamme, S., Cazalbou, J. B., Torres, F., and Chassaing, P., "Direct numerical simulation of the interaction between a shock wave and various types of isotropic turbulence," *Flow turbulence and combustion*, Vol. 68, 2002, pp. 227–268.

[81]Cohen, R. H., Dannevik, W. P., Dimits, A., Eliason, D., Mirin, A. A., Porter, D. H., Schilling, O., and Woodward, P. W., "Three dimensional high resolution simulations of Richtymyer Meshkov mixing and Shock Turbulence interaction," *6th International workshop on the physics of compressible turbulent mixing UCRL JC 125309*, 1997, pp. 6.

[82]Lee, S., *Interaction of isotropic turbulence with a shockwave*, Ph.D. thesis, Stanford university, 1992.

[83]Jackson, T. L., Hussaini, M. Y., and Ribner, H. S., "Shock-turbulence interactions in a reacting flow," *NASA ICase Report No. 92-20*, Vol. NASA CR- 189647, 1992, pp. 18.

[84]Jackson, T. L., Kapila, A. K., and Hussaini, M. Y., "Convection of a pattern of vorticity through a reacting shock wave," *Physics Fluids A*, Vol. 2, 1990, pp. 1260–1268.